The mini-GWAC optical follow-up of gravitational wave alerts – results from the O2 campaign and prospects for the upcoming O3 run

Damien Turpin[1], Chao Wu[1], Xu-Hui Han[1], Li-Ping Xin[1], Sarah Antier[2,3], Nicolas Leroy[2], Li Cao[1], Hong-Bo Cai[1], Bertrand Cordier[4], Jin-Song Deng (邓劲松)[1,5], Wen-Long Dong[1], Qi-Chen Feng[1], Lei Huang[1], Lei Jia[1], Alain Klotz[6,7], Cyril Lachaud[3], Hua-Li Li[1], En-Wei Liang (梁恩维)[8], Shun-Fang Liu[1], Xiao-Meng Lu[1], Xian-Min Meng[1], Yu-Lei Qiu[1], Hui-Juan Wang[1], Jing Wang (王竞)[8,1], Shen Wang[1], Xiang-Gao Wang (王祥高)[8], Jian-Yan Wei[1,5], Bo-Bing Wu[9], Yu-Jie Xiao[1], Da-Wei Xu[1,5], Yang Xu[1], Yuan-Gui Yang (杨远贵)[10], Pin-Pin Zhang[1], Ruo-Song Zhang[1], Shuang-Nan Zhang[1], Ya-Tong Zheng[1] and Si-Cheng Zou[1]

[1] Key Laboratory of Space Astronomy and Technology, National Astronomical Observatories, Chinese Academy of Sciences, Beijing 100101, China; *dturpin@nao.ac.cn*
[2] LAL, Univ. Paris-Sud, CNRS/IN2P3, Université Paris-Saclay, F-91898 Orsay, France
[3] APC, Univ Paris Diderot, CNRS/IN2P3, CEA/lrfu, Obs de Paris, Sorbonne Paris Cité, France
[4] CEA Saclay, DRF/IRFU/Département d'astrophysique, 91191 Gif-sur-Yvette, France
[5] School of Astronomy and Space Science, University of Chinese Academy of Sciences, Beijing 101408, China
[6] Université de Toulouse, IRAP 14 Av. Edouard Belin, F-31000 Toulouse, France
[7] Institut de Recherche en Astrophysique et Planétologie (IRAP), UPS-OMP, Toulouse, France
[8] Guangxi Key Laboratory for Relativistic Astrophysics, School of Physical Science and Technology, Guangxi University, Nanning 530004, China
[9] Institute of High Energy Physics, Chinese Academy of Sciences, Beijing 100049, China
[10] School of Physics and Electronic Information, Huaibei Normal University, Huaibei 235000, China

Abstract The second (O2) observational campaign of gravitational waves (GWs) organized by the LIGO/Virgo Collaborations has led to several breakthroughs such as the detection of GW signals from merger systems involving black holes or neutrons stars. During O2, 14 GW alerts were sent to the astronomical community with sky regions mostly covering over hundreds of square degrees. Among them, six were finally confirmed as real astrophysical events. Since 2013, a new set of ground-based robotic telescopes called Ground-based Wide Angle Camera system (GWAC) project and its pathfinder mini-GWAC has been developed to contribute to the various challenges of multi-messenger and time domain astronomy. The GWAC system is built up in the framework of the ground-segment system of the SVOM mission that will be devoted to the study of the multi-wavelength transient sky in the next decade. During O2, only the mini-GWAC telescope network was fully operational. Due to the wide field of view and fast automatic follow-up capabilities of the mini-GWAC telescopes, they were adept to efficiently cover the sky localization areas of GW event candidates. In this paper, we present the mini-GWAC pipeline we have set up to respond to GW alerts and we report our optical follow-up observations of eight GW alerts detected during the O2 run. Our observations provided the largest coverage of the GW localization areas with a short latency made by any optical facility. We found tens of optical transient candidates in our images, but none of those could be securely associated with any confirmed black hole – black hole merger event. Based on this first experience and the near future technical improvements of our network system, we will be more competitive in detecting the optical counterparts from some GW events that will be identified during the upcoming O3 run, especially those emerging from binary neutron star mergers.

Key words: gravitational waves — methods: data analysis — methods: observational — (stars:) gamma-ray burst: general

1 INTRODUCTION

The new generation of gravitational wave (GW) LIGO/Virgo detectors has given us access to new physics on compact and extreme objects in the Universe such as black holes (BHs) or neutron stars (NSs) with unprecedented detail, see for example Abbott et al. (2016a). In 2015, the O1 GW observational campaign marked the birth of GW astronomy with the first two detections of GW signals produced by the coalescence of black holes bounded in binary systems (a binary black hole, BBH) (Abbott et al. 2016b,c). A search for electromagnetic counterparts from these merger systems was performed without any significant result. While any electromagnetic counterpart from a BBH merger event is very unlikely, it has not been completely ruled out by some models under particular conditions (Loeb 2016; Zhang et al. 2016; Zhang 2016; Perna et al. 2016; de Mink & King 2017). In addition to that, the poor localization of these GW events and the long delay in alert communication dramatically reduced the detection capabilities of the electromagnetic facilities. From November 2016 to August 2017, the O2 run has been effective for almost one year with a release of 14 alerts to the external partners of the LIGO/Virgo Collaborations (LVC). This lead to new discoveries of GWs from compact mergers (Abbott et al. 2019). In particular, on 2017 August 17, the discovery of the GW signal GW170817 emitted, for the first time, from the inspiral and subsequent merger of two NSs (a binary neutron star, BNS) marked the dawn of multi-messenger astronomy (Abbott et al. 2017a,b,c). Two pieces of matter ejecta were identified after this merger. First, almost simultaneously with the GW signal, a short gamma-ray burst (sGRB), GRB 170817A (Goldstein et al. 2017), happened and much later its associated X-ray and radio afterglows that result from relativistic ejecta heated up its surrounding environment (for a review on sGRB, see Berger 2014, and references therein). Secondly, about 10 h after the GW trigger time, thanks to the intensive follow-up observations made by various optical facilities, an isotrotropic ejecta was also clearly identified as the signature of r-processes occurring in a so-called kilonova ejecta as predicted years ago by several authors (Li & Paczyński 1998; Kulkarni 2005; Metzger et al. 2010; Metzger 2017, for a recent review). GW170817 permitted validating for the first time the merger model proposed decades ago to explain the sGRB phenomenon (Paczynski 1986; Eichler et al. 1989; Paczynski 1991). Beyond this remarkable result, the O2 run demonstrated the importance of having a third detector operating at the Advanced Virgo facility, entering in science mode, to significantly reduce the error in localization of some GW events (Abbott et al. 2017a,d). However, the Virgo detector only joined the last month of the O2 run, thus, a large majority of the O2 GW candidates remained poorly localized. According to the online LVC detection pipeline, the median size of the sky localization error box of the O2 GW alerts was $\sigma_{90\%} = 1725 \deg^2$ (Abbott et al. 2019). Practically speaking, in the electromagnetic domain, with such localization constraint and depending on the distance to the event, the discovery potential of the telescopes having relatively small fields of view (FoVs, typically FoV <1 square degree (sq.deg)) and usually operating in pointing mode is very low. As a consequence, it was premature to conduct efficient electromagnetic follow-ups using optimized strategies for both small and wide FoV telescopes. The electromagnetic counterpart searches were therefore performed through various observational strategies including archival data analysis, prompt searches with all-sky instruments, wide-field tiled searches, targeted searches of potential host galaxies with small FoV facilities, and deep follow-up of individual sources. In the optical domain, wide field instruments have the advantage of being able to cover a large fraction of the GW error boxes in a minimum amount of time.

Since 2013, telescopes that are part of the Ground-based Wide field Angle Cameras (GWAC) have been under development at the Xinglong Observatory in China to prepare the future ground segment of the SVOM mission dedicated to study of the transient sky in 2021 with both spaced-based and ground-based multi-wavelength instruments (Wei et al. 2016). Due to the design of its extremely wide FoV ($25° \times 25°$), telescopes that are part of GWAC are well suited for the optical follow-up of GW candidates. They have the capability to perform routine observations of the transient sky every night and, being robotic, they are able to very rapidly cover a significant portion of the GW localization regions. These two attributes enabled us to conduct the first extensive optical follow-up of GW events, searching for early optical counterparts, from China. For the O2 GW run, our optical follow-up campaign was performed with the pathfinder telescopes associated with mini-GWAC. In this paper, we present our optical follow-up system of the O2 GW alerts and the results of our campaign. We will firstly describe, in Section 2, our mini-GWAC telescopes used during O2. We then present, in Section 3, our transient research program set up to respond to any multi-messenger alerts. The results of our follow-up observations of the GW alerts are presented in Section 4. In Section 5, we will discuss the improvements in our detection capabilities for the upcoming O3 run. Finally, we draw our conclusions in Section 6.

2 THE mini-GWAC TELESCOPES

In 2013, a GWAC pathfinder, called mini-GWAC, was developed in order to test and validate both the hardware and data processing pipeline of the future GWAC system.

Located at the Xinglong Observatory (lat = $40°23'39''$N, lon = $117°34'30''$E) and administered by National Astronomical Observatories, Chinese Academy of Sciences (NAOC), the mini-GWAC network is composed of six mounts. Each mount is equipped with two Canon 85/f1.2 cameras with an aperture of 7 cm, as displayed in Figure 1.

For each camera, the detector is a CCD Apogee U9000X[1] with an image cadence of 15 s (exposure=10 s, readout=5 s) and a readout noise of 12 electrons root mean square (RMS) at 1 MHz. Each camera is cooled down to $-45°$ C with respect to the local environment temperature with a thermoelectric cooler system with forced air. Two cameras are installed on a connector plate with a fixed angle and are covered in a rectangular sky field. With such a configuration, one mount has an FoV of 20 deg along the right ascension direction and 40 deg along the declination one. This results in an FoV of 800 sq.deg per mount. Combining the network of six mini-GWAC mounts, the overall FoV is about 5000 sq.deg. From the mini-GWAC single images, a typical limiting (unfiltered) magnitude of about 12 is obtained in a dark night without clouds. The mini-GWAC telescopes have been designed with an extremely wide FoV and a small imaging cadence in order to mainly search for short-time scale optical transients (OTs). The first light of mini-GWAC was obtained on October 2015 during the O1 GW science run and the first follow-up of a GW event was made for GW151226 (Wei et al. 2015). A specific data processing pipeline has been developed to automatically detect, in real-time, OT candidates in the images.

Each mini-GWAC telescope is operated in a sky survey mode. A pre-planned sky monitoring strategy is adopted, so that the whole sky is partitioned into several fixed grids whose sizes are based on each mount's FoV, see Figure 2.

During a night, each telescope starts to monitor one assigned sky grid until this one is no longer observable. For a given mount, each observed grid is chosen to optimize its observational conditions, i.e. a high elevation above the horizon, a minimum distance to the moon of $20°$ when the moon phase is lower than 0.5 (half moon, 1 is the full moon phase) and $30°$ otherwise and also having no overlap with the other grid pointings observed by other mini-GWAC telescopes. Once the first grids are no longer observable, the mounts automatically slew to observe new grids following the same observational strategy. Typically, no more than three different grids are usually monitored by a single mount in a single night. During the observations, each camera is automatically focused to provide the best image quality following the method developed by Huang et al. (2015). The images taken by all the mini-GWAC cameras are then analyzed in real-time and independently camera per camera.

3 THE mini-GWAC OPTICAL TRANSIENT SEARCH PROGRAM

During the mini-GWAC survey, we simultaneously conducted a program dedicated to the discovery of new OT sources in our images. This search program relies on two main steps: the detection of the OT candidates and then their classification using various filters. The OTs that can be detected in our mini-GWAC images originate from two classes of triggers: the external triggers such as the GW alerts or the internal triggers, i.e., the alerts produced by the GWAC system itself after the detection of an OT in real-time by chance in our images. Typically, in the external trigger case, we expect to catch the early phases of the GRB afterglow emission, some supernovae previously discovered by other groups, and galactic explosive events such as cataclysmic variables (CVs), tidal disruption events or the optical counterparts from GW events. For the internal triggers, we expect to rather detect near-Earth objects, uncataloged flaring stars, supernovae, galactic transients and also many unexpected OTs as the time-domain covered by mini-GWAC/GWAC (less than a minute timescale) is still as yet largely unexplored in the optical domain.

The analysis of the images is performed in real-time using two transient search methods, i.e., the catalog cross-matching method and difference image analysis (DIA). These methods usually yield the detection of dozens of OT candidates by each mini-GWAC telescope every night. In the following section, we briefly describe our two detection pipelines.

3.1 The Online mini-GWAC Data Processing

3.1.1 The catalog cross-matching method

A specific pipeline to detect short-living transients in the mini-GWAC images was developed mainly from the IRAF[2] package and SourceExtractor software (Bertin &

---

[1] More details on the CCD detector can be found here: *http://www.lulin.ncu.edu.tw/slt40cm/U9000.pdf*.

[2] IRAF is distributed by NOAO, which is operated by AURA, Inc., under cooperative agreement with NSF.
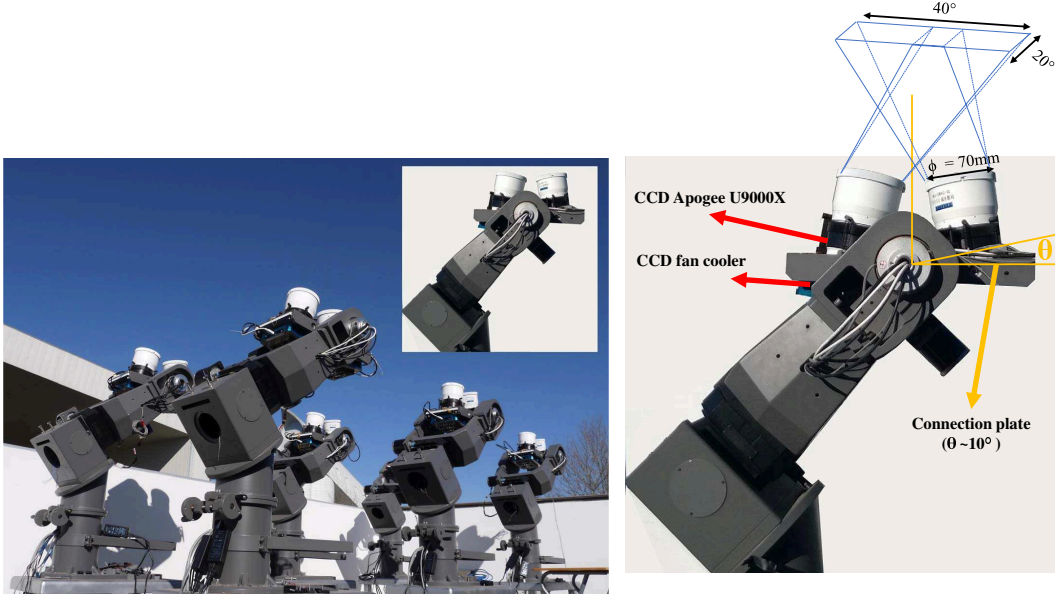
Fig. 1 (*left*) The mini-GWAC telescope farm, located at the Xinglong Observatory, which includes six mounts and 12 Canon 85/f1.2 cameras. (*Right*) Each mount is equipped with two cameras with an FoV of $20° \times 40°$ for a total FoV for the whole system of about 5000 sq.deg (about 1/4 of the northern sky). The image cadence is 15 s.
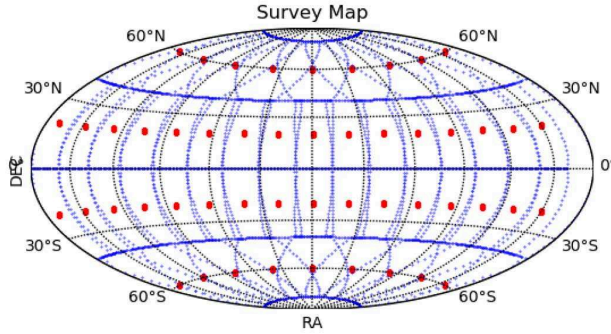
Fig. 2 The sky, in equatorial coordinates, partitioned into grids of equal area according to the mini-GWAC per mount's FoV. Each night, observations are performed in a survey mode following the grid pointings (*red dots*) with a maximum of three grids per mount to be visited. At the position of the Xinglong Observatory the grids with declination $\delta < 20°$ S are never observable.

Arnouts 1996). The method is based on a comparison of transient candidate positions found in the images with those of objects already cataloged in public archives. The catalog utilized in our pipeline is a mixture of the USNO B1.0 catalog and the stellar catalog produced by SourceExtractor using our reference images. The USNO B1.0 catalog was chosen because of its all-sky coverage with reasonable astrometric measurements and a high completeness down to $V = 16$, corresponding to the nominal design for the GWAC sensitivity. The reference images are obtained by co-adding 10 images with high quality from the same grid region. These images are automatically extracted in the mini-GWAC image database and selected based on the quality of their stellar point spread function (PSF), background brightness and atmospheric transparency. Note that the coma is quite serious at the extreme edge

of the mini-GWAC images which affects our detection efficiency. We estimated a loss of about 0.5 mag in our sensitivity threshold between OTs detected in the extreme edge of the image, where the PSF of stars can slightly deviate from a two-dimensional (2D) Gaussian profile, and the inner part of it (typically the 2k × 2k part of the image). A new optical source is detected in our images if it fulfills the following criteria:

(i) The candidate must not be detected in the reference image with a signal-to-noise ratio (SNR) greater than SNR = 5, but it is present in the night images.
(ii) In order to exclude some moving objects, the candidate should be detected in at least two continuous images without any apparent shift in its position.
(iii) There is no minor planet object with a brightness larger than 13 mag near the location of the candidate.

The choice of this limiting magnitude is made according to the sensitivity of the mini-GWAC telescopes.

(iv) There is no any defect in the CCD camera at the location of the candidate.

(v) The PSF and the ellipticity of any candidate should be a stellar-like profile (a 2D Gaussian profile with a limited deviation). At the edge of the image, this criterion reduces our detection efficiency for faint sources.

If an OT candidate is confirmed as being an uncataloged source, then our pipeline allows sampling the optical emission of the transient with a short time resolution of 15 s. In order to improve our detection capabilities, a stacking analysis based on a group of ten images is also processed in parallel. This allows increasing the SNR of faint objects to detect them at the edge of our camera sensitivity but with a lower time resolution. For these faint OTs, we will finally reach a time resolution from several minutes to a few hours.

3.1.2 Differential image analysis

The DIA is conducted by following three steps:

(i) an image alignment between the reference and the night images.

(ii) the difference between the two images to obtain a residual image.

(iii) the transient candidate selection after the residual analysis.

First, for the image alignment method, we used the Becker implementation[3] of the Alard (2000) algorithm finely tuned for the mini-GWAC data. All the images (reference and night) employed for DIA are truncated from the 3056×3056 px of the raw image to 2001×2001 px to avoid the bad PSF quality near the edge of the images. Before the subtraction, flux and PSF calibrations are applied to both images to obtain the best residuals possible. Once the subtraction is made, the transient selection program employs a supervised machine learning routine based on a random forest algorithm to preliminarily classify the spurious points in the residual images. The reference images are taken days before the trigger time to ensure, as much as possible, that no optical precursor is present in our data at the OT candidate position. Then, the OT selection criteria follow the same rules as the ones described above for the catalog cross-matching method. With such DIA method, we can also apply a stacking analysis in the images to enhance our optical flux sensitivity.

3.2 Optical Transient Classification

Once an image is processed, a list of preliminary OT candidates is automatically established by comparing the subsequent results of the two detection pipelines. These candidates, labeled as *OT1 candidates*, are usually composed of non-astrophysical sources, fake OTs such as minor planets or variable stars and a small amount of possibly genuine OT sources either in a rising or a fading phase.

The search for OTs then needs to carefully filter the OT1 candidates sample out of all the fakes through several steps. The first series of selection criteria mostly rely on the PSF analysis of the candidates, additional checks in other all sky catalogs such as 2MASS, SDSS9, DSS2, and their detection in a time series of at least two images. From this step, most of the *OT1 candidates* are mainly classified as non-astrophysical sources (i.e., hot pixels, crosstalk, cosmic rays, dust and CCD artifacts, moving debris, etc.) or astrophysical sources but identified as moving objects like minor planets. The candidates that pass these series of filters are then labeled as *OT2 candidates*, and the others are automatically rejected.

The *OT2 candidates* can still be a mix of fake OTs that were not filtered well during the first steps and few (or even zero) real OTs. Therefore, we analyze them one by one through a human-eye check (PSF matching, lightcurve and public archive check). For the candidates judged by our duty scientist as being promising, we trigger fast extra multiwavelength follow-up observations (Yang et al. 2019, in preparation) at deeper magnitudes (typically $R \sim 19$ for an exposure $= 120$ s) with two dedicated 60 cm robotic telescopes (GWAC-F60A/B, $UBVRI$ filters, jointly operated by NAOC and Guangxi University). Based on this set of information, we may confirm some of the *OT2 candidates* as being genuine OTs, while the others are finally rejected. The remaining confirmed OTs are therefore labeled *OT3 candidates*. At this stage, we usually reduce the initial number of candidates per night and per telescope from dozens to a very few (including zero) for the mini-GWAC system.

The *OT3 candidates* are automatically followed-up as long as possible during the night to better characterize the color evolution of their optical emission. According to the evolution of their lightcurves, we may associate some of these OTs with the astrophysical event (a GW merger event for example) that triggered such observations. If so, we will then publish an alert using the Gamma-ray Coordinates Network[4] and also quickly ask for spectroscopic follow-ups with the larger telescopes in China (for

---

[3] *http://www.astro.washington.edu/users/becker/v2.0/hotpants.html*

[4] *https://gcn.gfsc.nasa.gov* (GCN) system

example, the 2.16 m telescope at the Xinglong Observatory and the 2.4 m telescope at Lijiang Station of Yunnan Observatories). Such very promising OT candidates constitute our final sample labeled *OT4 candidates*. Our detection pipeline is summarized in Figure 3.
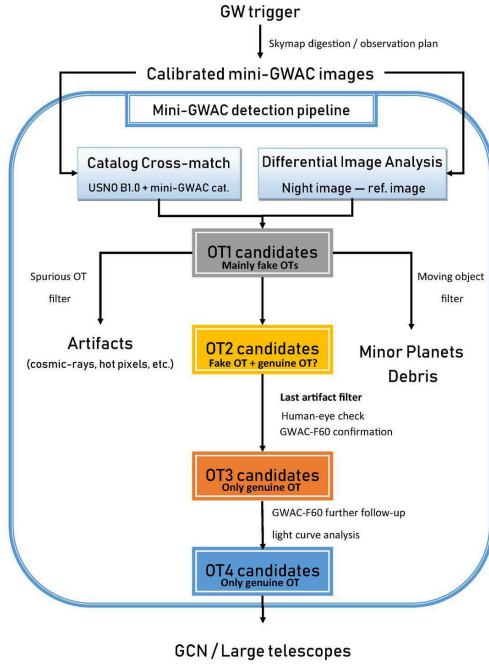
Fig. 3 A schematic view of the mini-GWAC detection pipeline for OTs. Our pipeline identifies the OT candidates through different steps through both automatic and human actions.

After our selection process, the transient candidates are classified into six categories in our database:

Category A / The sources are already cataloged: This category groups together the OT candidates that have finally matched the positions of known cataloged stars in the SIMBAD database (Wenger et al. 2000). This database is complete for the limiting magnitude of the mini-GWAC telescopes ($V = 12$).

Category B / The suspected variable/flaring stars: These OT candidates are tagged as variable stars when their positions match the ones of already cataloged variable stars and their lightcurve evolution is in good agreement with the ones of the associated variable stars.

Category C / The moving objects: The candidates are identified as moving objects by their tracks in several images or if they are already cataloged in the Minor Planet data center[5].

---

[5] *https://minorplanetcenter.net//iau/mpc.html*

Category D / The spurious points: This category groups together the OT candidates as being cosmic rays, instrument defects like hot pixels and noise in the residual images. The classification criteria are based on the occurrence rate of the source in our images. Typically, an OT candidate with an occurrence of less than twice in the image time series, associated historical data and the residual image is identified as noise.

Category E / The OTs with a host galaxy: This category groups the *OT3 candidates* that have matched, within a circle region of 90 arcsec around the mini-GWAC position (corresponding to $\sim$3 mini-GWAC pixels), the position of very nearby galaxies of the RC3 catalog (Corwin et al. 1994). This catalog is complete enough at the mini-GWAC limiting magnitude. This category actually may gather kilonovae (for the purpose of GW optical follow-up), supernovae, bright tidal disruption events, etc.

Category F / The host-less OTs: This category groups the *OT3 candidates* having no match with the RC3 galaxy catalog. Typically, these candidates may correspond to host-less astrophysical events or extra-galactic/cosmological events such as gamma-ray burst (GRB) afterglows.

3.3 Detection Efficiency of the mini-GWAC System

The OT search program has run for several years from 2014 to 2017 (not continuously) and is being updated every year. In this section, we aim to estimate the number of OTs the mini-GWAC telescopes are able to serendipitously detect in single frames according to our archival data. Our analysis is based on the latest period of mini-GWAC operation when the detection pipeline was upgraded to its last version so that the performances could be compared to the period covered by the O2 run. We selected six months of data between Oct. 2016 and Mar. 2017 which corresponds to a total of 1 673 607 images.

Within this period of archival data, 75 individual OT sources (typically flaring stars and a few unclassified astrophysical OTs) were detected by mini-GWAC in several hundred single frames. We therefore estimate that the expected number of new transients per single frame is on average $N_{OT/frame} = 4.5 \times 10^{-5}$ OT/frame. In other words, the mini-GWAC network is able to detect a new OT such as flaring stars brighter than $m_R \sim 12$ about every 11.5 d assuming that on average a night at Xinglong lasts 8 h. For a single camera, one night corresponds to about 1920 frames (including the readout time of 5 s for each frame). The OTs detected by one mini-GWAC camera can be considered as Poisson events in our sky sur-
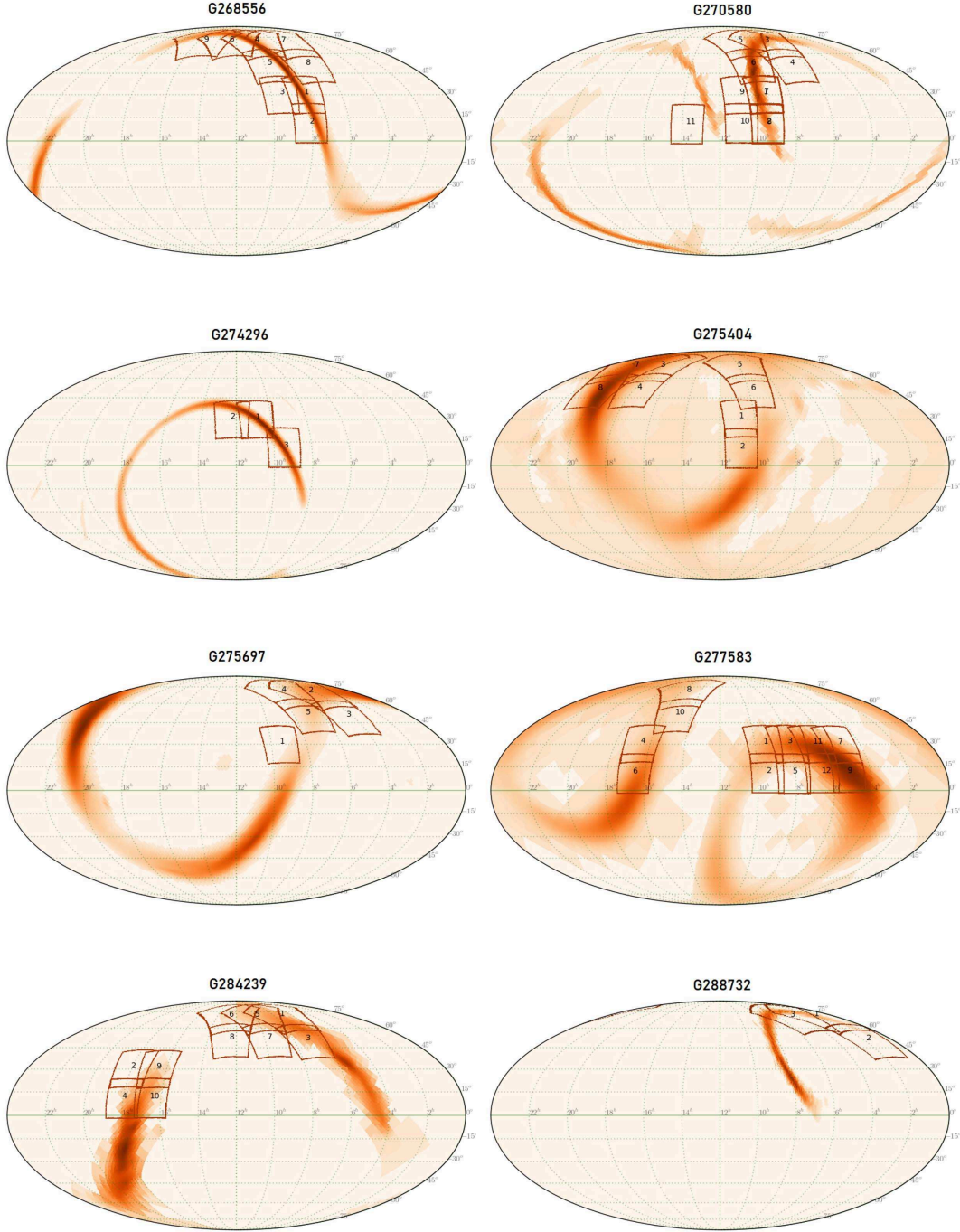
Fig. 4 The Bayesian probability skymaps of the eight GW events we followed-up during the O2 run. Our observation grids are marked with red squares, and are identified with a grid ID. All these grids were not necessarily scheduled at the same period because of observational constraints but they illustrate how we covered the GW error boxes throughout our periods of observation.

vey observations with a typical rate per night given by $\lambda = N_{OT/frame} \times 1920\,OT/night$. As a consequence, we estimate that the Poisson probability of detecting at least one OT, brighter than $m_R \sim 12$, during a night with one camera is $P[N_{OT,night} \geq 1|\lambda = 8.6 \times 10^{-2}] \sim 8.2\%$.

A single frame fills a sky pattern of about $400\,sq.deg$ which finally gives the number of OTs per sq.deg per frame exposure time one may expect to detect by chance with one

mini-GWAC camera

$$N_{OT/sq.deg/\Delta T_{frame}} = \frac{N_{OT/frame}}{FoV_{RA} \times FoV_{dec}}$$
$$= 1.1 \times 10^{-7} \, OT \cdot deg^{-2} \cdot \Delta T_{frame}^{-1},$$
(1)

where $\Delta T_{frame} = 10$ seconds and $FoV_{RA} = FoV_{dec} = 20°$. We emphasize that these statistics have to be taken as rough estimates of the mini-GWAC perfomances since they are averaged on very different observational conditions (weather, sky brightness, moon distance, airmass, duration of the observations per night, etc.) and random source positions in the images for which the detection efficiency can vary between the edge and the inner part of the image, see Section 3.1. However, these statistics give the right order of magnitude and will be useful for understanding the significance of any association of an OT detected in spatial coincidence with a GW event.

4 THE O2 FOLLOW-UP CAMPAIGN OF mini-GWAC

During the O2 GW observational campaign, 14 alerts were sent to the external partners of the LVC. The GW candidates were classified into two categories of potential astrophysical events able to emit GWs: compact binary mergers including BHs and/or NSs on one hand, and the collapse of a massive star or magnetar instability (Kotake et al. 2006; Ott 2009; Gossan et al. 2015; Mereghetti 2008) (mentioned as Burst) on the other hand.

The alerts with false alarm rates less than one per two months were distributed in the format of notices and circulars via private GCNs. The latency of the initial alert dissemination ranged from 30 min to a few hours due to the necessity of human validation of the data quality. Regular updates on the localization error box for the candidates were sent by LIGO/Virgo every few hours up to a few months. All the events were finally classified much later through an offline analysis performed by the LVC (Abbott et al. 2019). All of the confirmed events originated from compact binary mergers and except for GW170817, the only BNS merger, they were classified as BBH mergers.

4.1 Alert Reception System with mini-GWAC

The GW alerts were received through the GCN system as described in Abbott et al. (2019) and then recomposed in a VOEvent format. The GW Bayesian probability skymaps were decomposed using the predefined mini-GWAC sky grids. A list of tiles was therefore scheduled for observations by order of priority based on their respective probability of containing the GW event. The observation plan was composed for each telescope so that the different tiles could be observed several times during the night.

The recomposed alerts were produced by our French science center located at the Laboratoire de l'Accélérateur Linéaire (LAL) institute in Paris-Orsay and transmitted to the Chinese Science Center (CSC) at NAOC in Beijing that operates our telescopes at Xinglong Observatory. The message transfer connection was built with our own scripts developed in the Python language based on pub/sub mode of zeroMQ, which has features of authentication, encryption and validation of the messages. The connection protocol also supports automatic re-connection and re-sending of messages. The typical latency time is $\sim 0.16\,s$. Taking into account the additional delays due to the parsing and rewriting of a VOEvent alert as well as the response delay of the telescopes, the total latency for an alert received by mini-GWAC is typically less than 2 min.

4.2 Our Observations with mini-GWAC

During the O2 campaign, the mini-GWAC telescopes followed-up 8/14 GW alerts as demonstrated in Figure 4. The localized regions of the six other GW alerts were not visible at the Xinglong Observatory at all.

From our eight successful follow-ups, two of them (GW170104 and GW170608) were confirmed as GW sources originating from the inspiral and merger of two BHs. The six remaining events were later retracted (Abbott et al. 2019). The main results of our observational campaign are summarized in Table 1.

4.2.1 Response latencies to the O2 GW alerts

Except for two events (G275697 and G284239) where the weather conditions prevented us from observing as soon as the GW trigger was received, we responded with a short latency to the GW alerts, typically within a few minutes after the alert messages were received. We then continuously monitored the sky localization areas during several hours in the first night following the GW trigger times. For half of the followed-up GW alerts (G268556, G270580, G274296 and G275404), we were actually already observing a part of their sky localization areas during our survey program prior to receiving the alert (and even before the GW event for G275404), see Figure 5.

This highlights two major advantages of such wide FoV telescopes observing in survey mode. First, for a significant amount of alerts, they can make simultaneous (even prior for possible precursors) observations based on their regular observational schedule. This also prevents from having no prompt image in case of a failure

Table 1 Summary of the Observations Made at Xinglong Observatory During the O2 GW Run with the mini-GWAC Telescopes

GW triggers				mini-GWAC observations				
ID	Trigger date (UTC)	Loc. error (90%) deg^2	Confirmed/type	T_{start}	ΔT_{obs} (h)	$P_{GW,cov}$ on ΔT_{obs}	N_{OT2} (MP tag)	GCN Reference
(1)	(2)	(3)	(4)	(5)	(6)	(7)	(8)	(9)
G268556$^{(1)}$	2017–01–04 10:11:58	1630	Yes / BBH	T_{GW} + 2.3 h	∼10.0	62.4%	273 (2)	Wei et al. 2017a
G270580	2017–01–20 12:30:59.35	3120	No / Burst	T_{GW} + 20 min	∼9.5	53.8%	30 (1)	Wei et al. 2017b
G274296	2017–02–17 06:05:55.05	2140	No / Burst	T_{GW} + 6.3 h	∼5.0	63.8%	5 (3)	Wei et al. 2017c
G275404	2017–02–25 18:30:21	2100	No / NS-BH	T_{GW} − 5.5 h	∼9.0	31.7%	88 (3)	Wei et al. 2017d
G275697	2017–02–27 18:57:31	1820	No / BNS	T_{GW} + 2.7 d	∼7.0	6.4%	0	Wei et al. 2017e
G277583	2017–03–13 22:40:09.59	12140	No / Burst	T_{GW} + 12.5 h	∼10.0	46.2%	198 (8)	Wei et al. 2017f
G284239	2017–05–02 22:26:07.91	3590	No / Burst	T_{GW} + 2.6 d	∼8.0	22.0%	47 (0)	Xin et al. 2017
G288732$^{(2)}$	2017–06–08 02:01:16.492	860	Yes / BBH	T_{GW} + 15 h	∼2.5	18.5%	8 (0)	Leroy et al. 2017

Notes: The latency of the first image with the GW trigger time takes into account the GW alert transmission delay by the LVC to the multi-messenger community as well as the delay due to our own system and the local weather conditions. (3) See Abbott et al. (2019). (6) is the duration of the mini-GWAC observations related to each trigger. (7) is the Bayesian probability (integrated over our observation time) that the GW source is in our images based on the final release of the GW Bayestar skymap. (8) is the number of OT candidates (OT2) identified during ΔT_{obs} in the GW sky localization area (90% confidence level (C.L.)). None of these candidates were finally classified as real OTs and so none are credibly related to any GW event. The numbers of OT candidates identified as minor planets are indicated in parentheses. $^{(1)}$ renamed GW170104; $^{(2)}$ renamed GW170608.

of the alert receiver system. During our O2 campaign, we experienced two failures of our alert receiver system. G274296 had no impact on our follow-up as our mini-GWAC telescopes were actually already monitoring a sky area that covered the full GW error box visible at Xinglong Observatory. However, for G277583, we experienced an additional delay due to an internet connection loss to start our observations. Once the connection came back, we immediately pointed our mini-GWAC mounts to the GW sky regions.

On the other hand, some images can usually be taken a few hours or even days before the GW events in the survey mode, when little to no electromagnetic counterpart is expected. Therefore, the wide FoV telescopes have a considerable amount of reference images available for a large fraction of the sky which offers the possibility to make a quick vetting or confirmation of the OT candidates that may be found after some merger events by several other facilities.

### 4.2.2 Coverage of the GW sky localization area

From the GW Bayesian probability skymaps, we estimate that the median probability of having the GW events in our images during our periods of observation is 38.9%. For some events, mainly located in the northern hemisphere, our observations covered more than 60% of the Bayesian localization. This is the largest coverage (based on a GW localization of several thousand sq.deg) performed by any optical telescope on a single night during the O2 campaign. We also computed the real-time performance of our follow-up system concerning the coverage of the Bayesian probability skymaps as depicted in Figure 6.

During O2, our median instantaneous (based on periods of 1 h of observation) Bayesian probability coverage of the initial GW alert skymaps was $P_{cov,med} = 14.2\%$. This quantity is much more representative of the real capabilities of our mini-GWAC instruments to cover the GW localization area provided by only two interferometers (LIGO Handford and Livingston here). This demonstrates that despite the active participation of the wide FoV telescopes in the follow-up campaign, such as the mini-GWAC telescopes, improving the localization of the GW sky area is still crucial to optimize the scientific returns.

4.3 Results

The number of transient candidates found in our images and spatially correlated with the GW events depends on several parameters such as the size of the GW error box and our subsequent coverage of it, the duration of the observations in each grid as well as the local weather conditions (moon brightness, sky transparency, weather status, etc.). Taking these factors into consideration, we ended up with more than 200 OT2 candidates for G268556, but, for example, we could not detect any credible transient source in our follow-up of G275697 (having the poorest coverage of all the GW events in our sample). In Appendix A, we give the details of our observations, grid location per grid location, for each GW event. Our OT2 candidates are detected within a wide range of unfiltered magnitudes (calibrated in R-band Johnson Vega system) $m_R \in [12.3 - 6.8]$, see Figure 7.

Concerning the two confirmed BBH merger events, GW170104 and GW170608, none of our *OT2 candidates* (273 and 8, respectively) were classified as real OTs and hence, no OT3 candidates emerged from this step. All
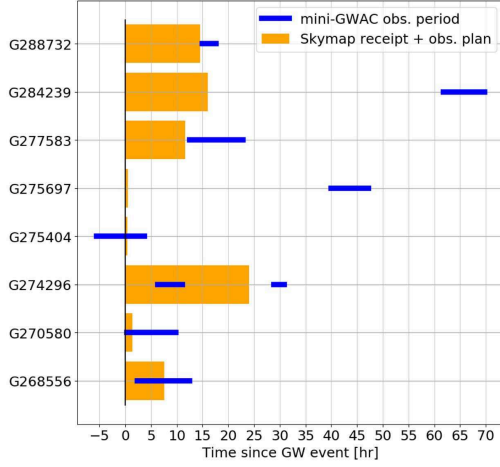
Fig. 5 The mini-GWAC response latencies to the GW alerts. For each GW event followed-up by mini-GWAC during O2, the *orange bars* correspond to the delivery time of the alert at the Xinglong Observatory. This delivery time is mainly due to the time for the LVC to send the circular alerts plus the time for our alert system to digest the GW skymap and produce an observation plan for mini-GWAC. The *blue bars* signify the period of our observations with respect to the GW trigger time.
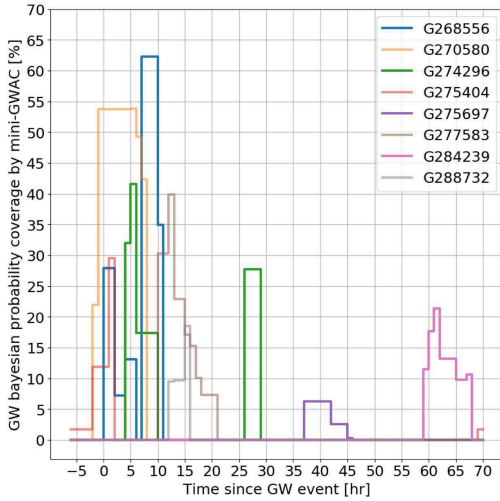
Fig. 6 The evolution of our eight GW skymap coverages (Bayesian probability) with mini-GWAC as a function of time expressed as the delay since the GW trigger time.

of our OT2 candidates were finally classified in category A (cataloged stars), category C (minor planets) as shown in Figure 8 or category D (spurious points). As a consequence, we could unambiguously reject any association with the two merger events. These null results can be explained both by observational constraints (sensitivity of our telescope, partial coverage of the GW error boxes) and by the physics of the BBH mergers that, if they truly radiate any electromagnetic emission, may power too faint of OT emissions to be detected by our set of telescopes.
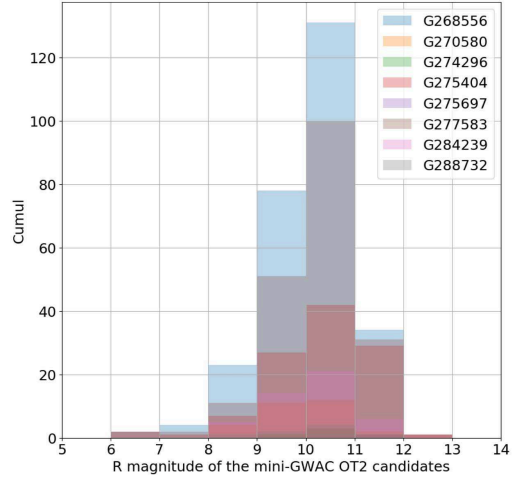

Fig. 7 Distribution of the R-band magnitude (unfiltered calibrated with the USNO B1.0 R2mag catalog) of the OT found in mini-GWAC images for each GW event. These magnitudes are computed at the time of detection for the OT candidates.

We compared these null results with the number of OTs we expected to find spatially correlated with the GW skymaps by chance in our period of observations. To do so, we used the following expression

$$
\begin{aligned}
\mathrm{N^{serendipitous}_{OT,GW}} =& N_{\mathrm{OT/sq.deg}/\Delta\mathrm{T_{frame}}} \\
& \times \mathrm{f_{GW}} \cdot \sigma^{90\%}_{\mathrm{GW}} \times \mathrm{N_{frame}} ,
\end{aligned}
\tag{2}
$$

where $\mathrm{N_{OT/sq.deg}/\Delta T_{frame}}$ has been defined in Equation (1), $\mathrm{f_{GW}}$ is the fraction of the GW skymap we covered in our observations, $\sigma^{90\%}_{\mathrm{GW}}$ is the contour of the GW probability skymap given at the 90% C.L. and $\mathrm{N_{frame}}$ is the number of single frames we took during our periods of observation. For each GW event, we actually computed this expression for every single tile covering a portion of the skymap during a certain amount of time, see our observation log in Appendix A. For a given GW event, the final result is the addition of the expectations given in all the individual tiles for those that predict at least one event. Otherwise, if none of the tiles predict any OT detection, we took the best expectation among all the tiles. Concerning our observational campaign of the two BBH mergers GW170104 and GW170608, we finally end up with $\mathrm{N^{serendipitous}_{OT,GW}} \sim 2.6 \times 10^{-2}$ and 6.0×10^{-3} expected OTs, respectively. These estimates highlight the fact that any single OT detected in spatial coincidence with any of these two GW events would have been of very great interest, as a serendipitous OT detection by the mini-GWAC telescopes is strongly unfavored. For completeness, we compute the same estimates for all the GW alerts we followed-up and summarize the results in Table 2. We tentatively set an upper limit (U.L.) on the
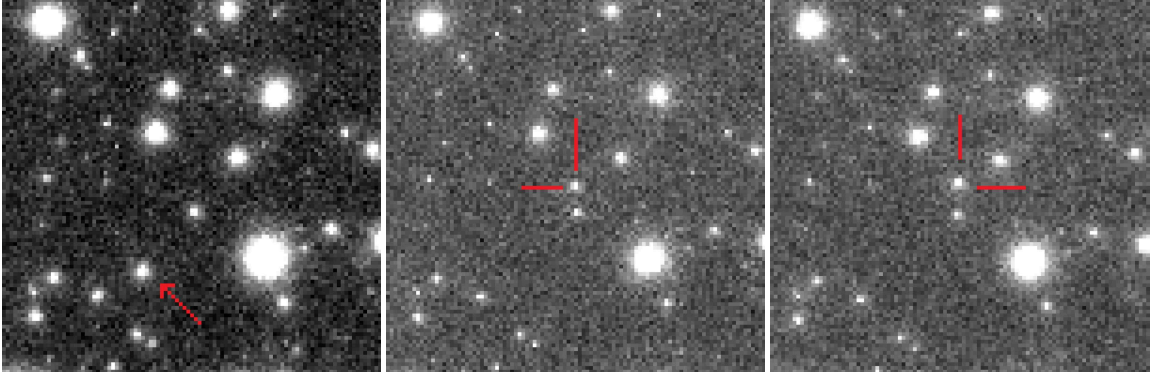
Fig. 8 The reference (*left*) and the first and last night images (*middle* and *right* respectively) of a moving object detected by mini-GWAC during our follow-up of G274296 on 2017-02-17 12:18:28 ($V = 11.1$ mag). Note that this minor planet (471 Papagena) is also present in the reference image (*red arrow*) a day before with an angular distance of about 13 arcmin with respect to its position measured during our observations.

Fig. 9 (*Left*) The GWAC observation system mounted on its test bench at the Xinglong Observatory. O3 will be composed of four mounts. The total FoV of such a configuration is about 2000 sq.deg. The imaging time resolution is 15 sec for single frames. (*Center*) Two GWAC-F60 telescopes (60 cm) are employed to quickly confirm GWAC OTs and perform deeper follow-up observations if needed. (*Right*) A 30 cm telescope (GWAC-F30) will also be operated during the O3 campaign (FoV $= 1.8° \times 1.8°$).

Table 2 Comparison study between the number of OTs we may expect to detect during our follow-up campaign and those we actually detected. For each GW event, no OT has been found, in agreement with our expectations. As a consequence, one OT detection would immediately lead to a strong probability of association with the real GW merger events (G268556 and G288732).

GW event	$N_{OT,GW}^{ser.}$ / (OT detected)
G268556	2.6×10^{-2} / (0)
G270580	1.6×10^{-1} / (0)
G274296	3.5×10^{-2} / (0)
G275404	6.8×10^{-3} / (0)
G275697	7.7×10^{-3} / (0)
G277583	1.5×10^{-1} / (0)
G284239	4.4×10^{-2} / (0)
G288732	2.6×10^{-2} / (0)

optical flux of GW170104 during our period of observations but under the hypothesis that the event was located in the portion of the sky we monitored. This 3σ U.L., lying in the range $m_R \in [12.3 - 11.4]$, varies from one grid to another as the sky brightness can significantly change. For GW170608, the limiting magnitude of our images is less stringent because of a cloudy sky. The optical flux U.L. of

GW176008 finally lies in the range $m_R \in [10.9 - 9.9]$, again assuming that the event was localized in our images.

5 TOWARDS THE NEXT LIGO-VIRGO O3 RUN

The next GW scientific run on April 2019 (O3) also promises to be prolific in terms of the number of GW detections that will need extensive electromagnetic follow-up campaigns. Thanks to the sensitivity improvement of the LIGO-Virgo detectors, one can expect, in the most optimistic scenario, one BNS merger per month and most likely a few BBH mergers per week. The localization uncertainties of the GW O3 events will be largely reduced due to the combination of the LIGO-Virgo detectors with a median localization region comprised in the range 120–170 deg^2 within the 90% C.L. contours for LIGO only[6]. Despite such significant improvement in the localizations, the need for wide FoV telescopes will be still crucial for some events. Furthermore, according to the expected high GW alert rate, the availability of worldwide networks of

---

[6] See the LIGO/Virgo prospects for the O3 run here `https://emfollow.docs.ligo.org/userguide/capabilities.html\#livingreview` and the associated references.

telescopes dedicated to the electromagnetic follow-up of such GW events will be a key factor to make the O3 run as much of a scientific success as O2 was.

5.1 From the mini-GWAC to the GWAC System

Since the end of 2017, mini-GWAC have been totally replaced by the nominal design of telescopes for the GWAC and are no longer used. Each GWAC mount is equipped with five cameras (four × Joint Field of View cam (JFoV) camera: 4k × 4k CCD E2V camera with an aperture of 180 mm each + one Full Field of View cam (FFoV): 3k × 3k CCD camera with an aperture of 35 mm), see Figure 9. With such a system, each mount will have an FoV of about $25° × 25°$ ($\sim$500 sq.deg) with an optical flux coverage extending from $V \sim 6$ magnitude up to 16 magnitude[7] in the visible domain, $\lambda \in$ [500–850 nm]. As for mini-GWAC, an image cadence of 15 s is set. For the O3 run, four GWAC mounts will be available at the Xinglong Observatory[8]. We summarize, in Table 3, some parameters of the GWAC telescopes and compare them with those of the mini-GWAC telescopes to highlight the improvements. The major improvements are the increase of the GWAC sensitivity and the angular resolution compared with the mini-GWAC system.

In association with the GWAC telescopes, our two fully robotized 60 cm telescopes (GWAC-F60A/B) will also be utilized to automatically confirm the genuineness of the GWAC OT candidates with a localization accuracy of the source of $\sigma \sim 1$ arcsec. They will also provide multi-wavelength (Johnson $UBVRI$) observations of the galaxies targeted in the GW probability skymaps. Finally, the GWAC system will be completed by the GWAC-F30 robotic telescope (30 cm) operated with a substantial FoV of $1.8° × 1.8°$ using different filters (Johnson $UBVRI$). As a whole, this GWAC system offers multiple capabilities of observations and strategies for the optical follow-up of GW alerts.

5.1.1 Real-time stacking analysis and search for slow transients

Once data will be taken, we will conduct a stacking analysis of our images to reach a maximum sensitivity of $V \sim 18$ (a gain of six magnitudes with respect to the mini-GWAC system) with a time-resolution of several

hours while keeping a high imaging quality as depicted in Figure 10.

This kind of set-up is built to search for moderately slow fading and faint transients having low SNRs in our single images. The stacking analysis of GWAC images would permit reaching the detection threshold of kilonova optical emission near its maximum brightness if such events are as close and bright as AT 2017gfo, the kilonova optical counterpart of the BNS merger GW170817 ($m_{R,peak} \sim 17.2$). The discovery potential of GRB optical afterglow emission is also highly enhanced with such increase in our sensitivity. However, in the case of the GRB afterglows, the geometry of the emission can significantly affect our detection capability, whether the electromagnetic emission is isotropically radiated or through a narrow jet. If a jet is involved, its viewing angle will also play a significant role. If it is seen largely off-axis compared to our line of sight, the electromagnetic flux we may receive will be strongly reduced and delayed, hence disfavoring an optical detection by our telescopes. On the contrary, for a jetted emission seen on-axis at the BNS distance range of LIGO-Virgo for O3 (120 Mpc – 60 Mpc), we will very likely detect the optical emission that is expected to be significantly brighter than the GWAC sensitivity ($R = 16$ mag) at early time post merger.

5.1.2 Automatic and quick classification of the transient candidates

A key challenge of relying on wide FoV telescopes is the ability to quickly identify and classify the numerous transient sources they detect each night. Despite the FoV of the mini-GWAC telescopes being very large, their limiting sensitivities prevented them from detecting a huge number of OTs every night (a few dozens of OT candidates per mount). Therefore, it was still possible that humans were fully involved in the process of source classification. For GWAC, this will be no longer the case as the sensitivity of each mount is significantly increased and especially considering the real-time stacking analysis. Typically, in one dark night, the GWAC detection pipeline can be triggered (at the very basic level of OT1) hundreds of times with only single images and the cameras on one mount. As explained in Section 3.1, the preliminary sample of OT candidates is usually composed of artifacts and possibly a few genuine astrophysical sources. A new method of OT classification has been developed in the framework of the GWAC data processing pipeline based on a machine learning approach. This new classification method, that will be described in detail in a separate paper, will implement Convolutional Neural Networks (CNN). This approach is now widely

---

[7] This sensitivity is reached during a dark night for 10 seconds of exposure.

[8] At completion, the GWAC network system will be composed of a set of 10 mounts located in China and 10 others located outside of China (the second site is still under discussion).

Table 3 Comparison between Some Parameters of mini-GWAC and GWAC

Parameter	mini-GWAC value	GWAC value	GWAC improvement factor
Network FoV (sq.deg)	5000	5000	1
Tel. diameter (cm)	7.0	18 (JFoV)	~ 2.5
Pixel size (μm)	12	13	~ 1
Pixel scale (arcsec)	29.5	11.7	2.5
Readout noise (e^-)	10	14	0.7
FWHM (center)	1.2	1.5	1.25
R_{lim} (mag/single frame)	12	16	~ 40 (in flux sensitivity)
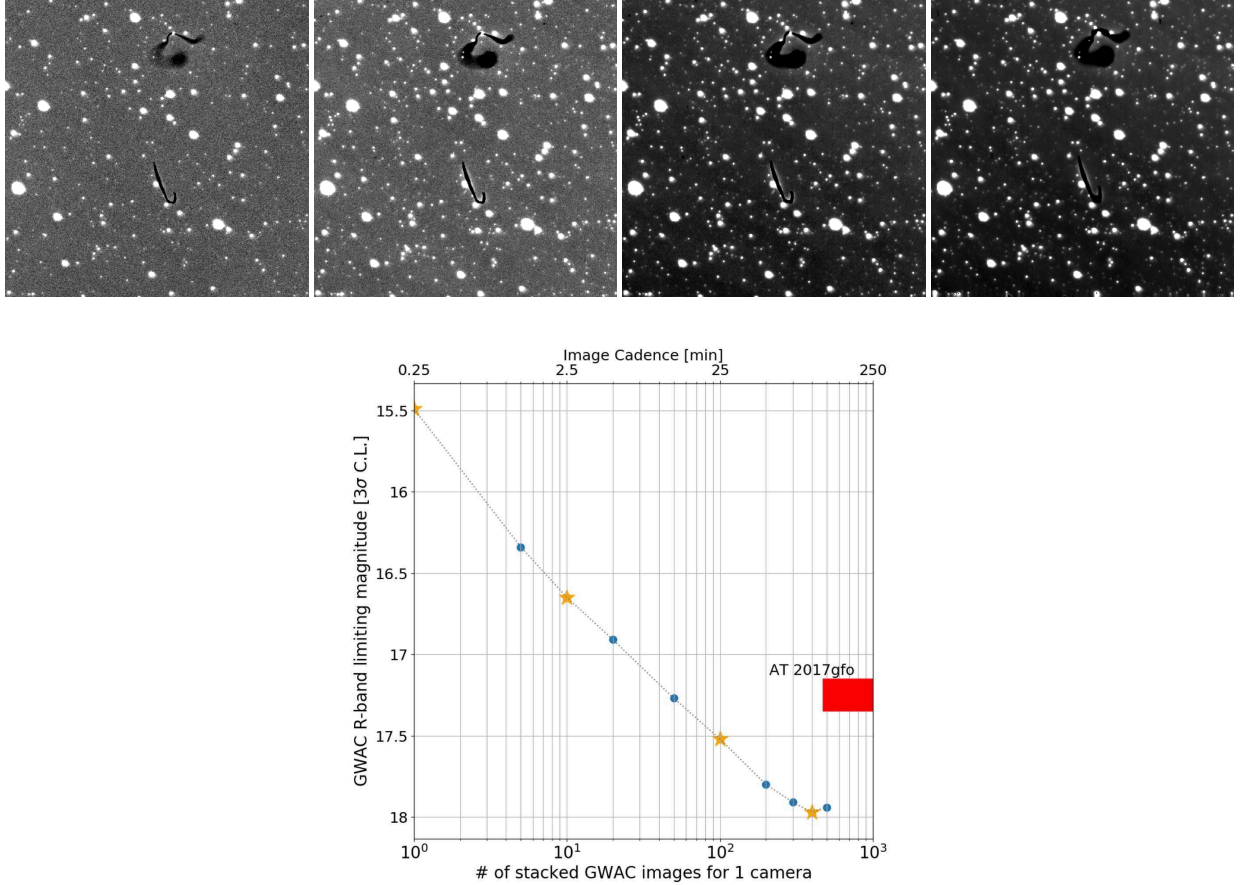
Fig. 10 (*Top*) Series of stacked GWAC sub-images using N = 1 (single image), 10, 100 and 400 images, respectively from left to right. From the left to the right images, the limiting magnitude goes from $R = 15.49$ to $R = 17.97$ (calibrated with the USNO B1.0 R2mag stars). (*Bottom*) Limiting magnitudes of GWAC (3σ C.L.) as a function of the number of stacked images. The *orange stars* represent the limiting magnitude of the GWAC images displayed above. The kilonova (AT 2017gfo) associated with the GW170817 event is shown assuming a minimum typical timescale of 10 h for the optical emission. Our stacking analysis would allow us to reach the detection threshold for such kind of event.

adopted for telescopes having wide FoVs (e.g., Gieseke et al. 2017; Sánchez et al. 2019; Mahabal et al. 2019; Jia et al. 2019) and is particularly efficient in detecting bogus sources in images such as cosmic rays, hot pixels, etc. (category D of our own classification ranking, see Section 3.2), which constitute the major fraction of our false detections at the OT1 level. The goal is to filter out around 95% of the false positives detected in our *OT1 candidate* sample. It is crucial for such telescopes in order to be efficient in detect-

ing "the good ones" and to ensure that our OT candidates will be of great interest for the astronomical community when we will release public GWAC alerts.

5.1.3 The first training of the SVOM ground follow-up system.

In 2021, the SVOM mission will be complimented by a network of ground optical/near-infrared telescopes devoted to the follow-up of SVOM triggers or target-of-opportunity

triggers approved by the SVOM Collaboration (Wei et al. 2016). At completion, this ground segment should be composed of the SVOM/COLIBRI telescope located at the Observatory of San Pedro Mártir (Mexico), a set of ten GWAC mounts sited outside of China (the location is still under discussion) and some telescopes placed inside of China: ten GWAC mounts, two GWAC-F60, one GWAC-F30 and the C-GFT telescope (1.2 m). For the O3 run, only the Chinese part of the SVOM segment will be available with four operational GWAC telescopes and also including the C-GFT telescope. The goal of this Chinese network is to cover the GW skymap in the most efficient way by combining different observational strategies such as tiling observations of the GW skymap or galaxy targeting. This strategy will take into account the individual characteristics of our telescopes that will be connected to the SVOM CSC for O3 at NAOC. The CSC will be in charge of collecting all the observational results and producing the public reports. This centralized database system will allow us to execute our strategy almost in real time depending on whether we need to explore new fields, make some revisit observations or confirm OT candidates with multi-band photometric observations. With such a system, we will provide, as fast as possible and publicly through the GCN network, the list of the most interesting OT candidates we have identified: the so-called *OT4 candidates* according to our internal labeling system described above. In order to better characterize these promising OTs, based on their temporal behavior and their color evolution, we will conduct spectroscopic follow-up observations using the 2.16 m telescope at the Xinglong Observatory and the 2.4 m telescope at the Lijiang Station of Yunnan Observatories. Note that we can also perform deep color photometry with such telescopes with a limiting magnitude $B/V/R \sim 22$ for 10 min exposure time (under an airmass = 1.3) with the BFOSC instrument mounted on the 2.16 m telescope (Fan et al. 2016). For the same exposure time, we can reach an $R \sim 24$ limiting magnitude with the 2.4 m telescope. During the O2 run, we performed such deep follow-up observations with the 2.16 m telescope at Xinglong Observatory for an OT detected by Swift/UVOT related to the GW trigger G299232 (Meng et al. 2017). We could not detect this transient down to a magnitude $r \sim 22$, confirming its fading behavior compared to the Swift/UVOT data and consistent with observations performed by other teams. This example shows how these moderately large telescopes will allow us to extend our follow-up capabilities for faint sources ($r < 22$) to possibly detect sources similar to the GW170817/AT 2017gfo kilonova (Villar et al. 2017) days after the merger event.

6 CONCLUSIONS AND PERSPECTIVES

The O2 GW observational campaign has opened a new window to study extreme objects in the Universe. It helped us to validate the capability of the mini-GWAC telescope network as being a fast follow-up system dedicated to multi-messenger astronomy. So far, our O2 observational campaign represents the largest coverage of the GW sky localization areas made by optical telescopes with short latencies. No credible OT was found in our images which we attribute to two main reasons. First, the confirmed GW events we have followed-up were all originating from BBH mergers from which electromagnetic emission is highly uncertain. Secondly, the sensitivity of the mini-GWAC telescopes ($m_R = 12$) was too low to detect faint transient sources such as the kilonova emission like the one observed for GW170817/AT2017 gfo or any GRB afterglow emission. Based on this experience, we have presented our new plan for the upcoming O3 run. We showed the improvement of our observational capabilities by combining both a migration from the mini-GWAC to the GWAC system, with a much higher sensitivity in the visible domain, and the extension of our network will permit us to be more competitive in our searches for optical counterparts from GW events, especially those emerging from BNS mergers. The O3 run will also be a unique opportunity to build the first blocks of the ground follow-up system of the future SVOM mission that integrates the GWAC system.

Appendix A: THE LOG. TABLES OF THE mini-GWAC OBSERVATION PERFORMED FOR EIGHT GW EVENTS DURING THE O2 LIGO/VIRGO RUN

Table A.1 The Observation Logs of the Mini-GWAC Follow-up of G268556 (trig. Date: 2017–01–04 10:11:58)

mini-GWAC grid / cam ID	T_{start} 2017-01-04	T_{end} 2017-01-04	mid time (hour)	center RA (h:m:s)	center dec (deg:m:s)	$P_{GW,cov}$	N_{im} / N_{OT2}	$M_{R,OT2}$ [min - max]
1 / C1	12:30:41.1	13:49:41.5	T_{GW} + 2.9704	07:46:49.578	+29:35:33.46	18.5%	316 / 50	[12.3 – 8.7]
2 / C2	12:30:41.1	13:49:49.5	T_{GW} + 2.9715	07:48:54.239	+10:34:56.09	13.4%	317 / 36	[11.9 – 8.2]
3 / C1	13:50:29.3	15:14:52.1	T_{GW} + 4.3452	09:10:51.599	+29:36:54.60	3.1%	338 / 0	–
7 / C5	14:55:58.2	17:57:22.7	T_{GW} + 6.2451	06:34:42.357	+69:28:01.79	3.9%	726 / 0	–
8 / C6	14:56:10.4	17:57:35.7	T_{GW} + 6.2486	06:40:16.529	+50:28:28.89	0.3%	726 / 0	–
6 / C3	16:21:28.7	17:57:31.9	T_{GW} + 6.9590	11:52:01.006	+70:06:03.83	11.0%	384 / 0	–
4 / C1	19:14:27.3	22:39:37.7	T_{GW} + 10.7513	09:17:21.644	+69:37:03.40	17.7%	821 / 142	[11.4 – 6.8]
5 / C2	19:14:27.3	22:39:25.3	T_{GW} + 10.7495	09:21:25.794	+50:35:59.26	16.7%	820 / 1	9.9
6 / C5	19:14:32.9	22:39:31.9	T_{GW} + 10.7512	11:52:01.006	+70:06:03.83	11.0%	820 / 159	[11.4 – 6.8]
1 / C3	19:14:39.9	21:17:22.8	T_{GW} + 10.0676	07:46:49.578	+29:35:33.46	18.5%	490 / 2	[11.1 – 10.5]
2 / C4	19:14:39.9	21:17:36.8	T_{GW} + 10.0695	07:48:54.239	+10:34:56.09	13.4%	492 / 24	[11.1 – 8.3]
9 / C7	19:14:55.3	22:39:18.3	T_{GW} + 10.7524	14:34:10.239	+70:01:52.84	7.1%	818 / 110	[11.4 – 6.8]

The time of each observation is given in UTC. T_{start} and T_{end} correspond to the interval time during which the mini-GWAC telescopes were taking images (with a cadence of 15 s). The mid time of the whole mini-GWAC observations is computed in the interval [$T_{start} - T_{end}$]. The RA and dec coordinates of the images stand for the center of each image (FoV $\sim 20° \times 40°$). The number of images as well as the number of OT candidates detected during the whole observation period is given for information with N_{im} and N_{OT2}, respectively. Note that several OT candidates might be detected by different cameras as there are significant overlaps between the observed fields. Finally, $M_{R,OT2}$ corresponds to the range of magnitudes where the OT candidates were found in single images (unfiltered calibrated with R/Johnson). These are also applied in Tables A.2, A.3, A.4, A.5, A.6, A.7 and A.8.

Table A.2 The Observation Logs of the Mini-GWAC Follow-up of G270580 (trig. date: 2017–01–20 12:30:59.35)

mini-GWAC grid / cam ID	T_{start} 2017-01-20	T_{end} 2017-01-20	mid time (hour)	center RA (h:m:s)	center dec (deg:m:s)	$P_{GW,cov}$	N_{im} / N_{OT2}	$M_{R,OT2}$ [min - max]
1 / C1	12:50:28.3	14:15:07.6	T_{GW} + 1.0302	09:10:23.301	+29:35:57.71	16.2%	339 / 1	8.6
2 / C2	12:50:28.3	22:14:58.6	T_{GW} + 5.0289	09:12:26.259	+10:35:26.10	8.3%	2258 / 0	–
3 / C5	13:50:51.4	19:47:59.1	T_{GW} + 4.3072	06:36:32.060	+69:30:22.27	12.7%	1429 / 20	[11.7 – 9.6]
4 / C6	13:50:51.4	19:48:01.2	T_{GW} + 4.3072	06:42:03.137	+50:31:15.23	0.2%	1429 / 0	–
5 / C1	14:15:35.4	22:19:45.5	T_{GW} + 5.7781	09:17:48.639	+69:36:41.75	12.9%	1937 / 6	[11.8 – 10.2]
6 / C2	14:15:35.4	22:19:48.5	T_{GW} + 5.7785	09:21:16.884	+50:34:54.73	23.0%	1937 / 2	[10.3 – 10.2]
1 / C3	14:16:01.4	21:24:39.2	T_{GW} + 5.3224	09:08:57.610	+30:01:54.06	16.4%	1715 / 4	[11.8 – 8.4]
2 / C4	14:16:01.4	21:25:03.9	T_{GW} + 5.3259	09:13:11.448	+09:57:30.75	8.0%	1716 / 3	[11.5 – 11.1]
9 / C5	19:49:04.7	21:36:13.2	T_{GW} + 8.1943	10:34:34.322	+29:30:16.35	5.3%	429 / 1	8.4
10 / C6	19:49:27.9	22:19:41.5	T_{GW} + 8.5598	10:37:18.165	+10:30:56.78	0.1%	601 / 0	–
11 / C4	21:32:19.1	22:19:53.1	T_{GW} + 9.4185	13:29:12.042	+10:00:17.26	0.1%	190 / 0	–

Table A.3 The Observation Logs of the Mini-GWAC Follow-up of G274296 (trig. date: 2017–02–17 06:05:55.05)

mini-GWAC grid / cam ID	T_{start} 2017-02-17	T_{end} 2017-02-17	mid time (hour)	center RA (h:m:s)	center dec (deg:m:s)	$P_{GW,cov}$	N_{im} / N_{OT2}	$M_{R,OT2}$ [min - max]
1 / C1	12:20:29.0	13:45:04.7	T_{GW} + 6.1144	10:34:48.326	+29:29:08.60	32.0%	338 / 4	[12.2 – 8.5]
2 / C1	13:45:30.2	17:12:33.6	T_{GW} + 8.5519	11:58:53.431	+29:29:28.69	17.4%	828 / 1	9.6
3 / C6†	10:53:52.3	12:57:00.8	T_{GW} + 28.9920	09:12:10.933	+10:39:50.19	27.7%	493 / 0	–

† For this set of observations the corresponding date is 2017–02–18.

Table A.4 The Observation Logs of the Mini-GWAC Follow-up of G275404 (trig. date: 2017–02–25 18:30:21)

mini-GWAC grid / cam ID	T_{start} 2017-02-25	T_{end} 2017-02-25	mid time (hour)	center RA (h:m:s)	center dec (deg:m:s)	$P_{GW,cov}$	N_{im} / N_{OT2}	$M_{R,OT2}$ [min - max]
5 / C7	13:01:04.2	21:37:38.1	T_{GW} − 1.1832	09:21:25.5	+69:40:01	1.4%	2066 / 0	–
6 / C8	13:01:04.2	21:37:39.7	T_{GW} − 1.1831	09:23:01.6	+50:00:25	0.4%	2066 / 1	12.0
1 / C3	19:23:51.9	20:41:04.7	T_{GW} + 1.5354	10:33:59.6	+30:12:22	0.5%	309 / 2	[11.6 – 9.2]
2 / C4	19:23:51.9	20:41:06.2	T_{GW} + 1.5356	10:38:05.6	+10:07:57	1.8%	309 / 50	[12.1 – 5.3]
3 / C5	19:23:42.2	22:13:19.6	T_{GW} + 2.3027	17:18:04.0	+69:28:00	6.9%	678 / 32	[12.2 – 10.4]
4 / C6	19:23:44.7	22:13:38.0	T_{GW} + 2.3057	17:21:47.1	+50:28:32	2.0%	680 / 4	[11.9 – 11.8]
7 / C7	21:39:38.3	22:13:28.5	T_{GW} + 3.4368	20:00:36.6	+69:38:42	12.5%	135 / 0	–
8 / C8	21:39:38.3	22:13:25.5	T_{GW} + 3.4364	20:01:12.7	+50:00:21	16.4%	135 / 0	–

Table A.5 The Observation Logs of the Mini-GWAC Follow-up of G275697 (trig. date: 2017–02–27 18:57:31)

mini-GWAC grid / cam ID	T_{start} 2017-03-01	T_{end} 2017-03-01	mid time (hour)	center RA (h:m:s)	center dec (deg:m:s)	$P_{GW,cov}$	N_{im} / N_{OT2}	$M_{R,OT2}$ [min - max]
1 / C1	10:55:43.4	18:11:04.6	$T_{GW} + 43.5981$	09:10:04.5	+29:30:47	0.3%	1741 / 0	–
2 / C3	10:55:26.9	14:04:55.7	$T_{GW} + 41.5445$	03:52:34.0	+68:53:23	5.0%	758 / 0	–
3 / C4	10:55:26.9	14:04:55.7	$T_{GW} + 41.5445$	04:02:12.2	+48:48:08	0.4%	758 / 0	–
4 / C5	10:55:24.5	17:44:07.8	$T_{GW} + 43.3709$	06:34:55.5	+69:32:01	1.5%	1635 / 0	–
5 / C6	10:55:24.5	17:44:07.8	$T_{GW} + 43.3709$	06:40:15.5	+50:32:35	1.3%	1635 / 0	–

Table A.6 The Observation Logs of the Mini-GWAC Follow-up of G277583 (trig. date: 2017–03–13 22:40:09.59)

mini-GWAC grid / cam ID	T_{start} 2017-03-14	T_{end} 2017-03-14	mid time (hour)	center RA (h:m:s)	center dec (deg:m:s)	$P_{GW,cov}$	N_{im} / N_{OT2}	$M_{R,OT2}$ [min - max]
9 / C6	11:10:11	13:33:39	$T_{GW} + 13.6959$	04:58:00.5	+10:28:12	19.2%	574 / 35	[11.5 – 7.6]
1 / C1	11:10:29	17:59:02	$T_{GW} + 15.9100$	09:10:29.8	+29:50:17	2.4%	1634 / 18	[12.2 – 9.1]
7 / C5	11:10:30	13:33:01	$T_{GW} + 13.6933$	04:55:10.8	+29:25:59	7.3%	570 / 41	[11.7 – 8.9]
3 / C3	11:10:45	16:40:29	$T_{GW} + 15.2576$	07:46:15.6	+29:57:47	6.2%	1319 / 16	[12.0 – 6.8]
5 / C4	11:10:45	16:40:01	$T_{GW} + 15.2537$	07:50:25.4	+09:54:53	1.1%	1317 / 9	[11.8 – 9.8]
2 / C2	11:10:55	17:59:54	$T_{GW} + 15.9208$	09:13:10.6	+10:17:08	1.0%	1635 / 4	[11.4 – 9.9]
12 / C8	12:45:01	15:56:16	$T_{GW} + 15.6747$	06:20:02.3	+10:21:24	8.2%	765 / 52	[11.8 – 9.3]
11 / C7	12:45:41	14:56:37	$T_{GW} + 15.1832$	06:18:37.7	+29:46:06	11.5%	524 / 22	[11.6 – 8.9]
10 / C6	13:34:09	21:30:00	$T_{GW} + 18.8653$	14:40:07.7	+50:29:58	0.4%	1903 / 0	–
8 / C5	13:34:31	21:30:00	$T_{GW} + 18.8683$	14:36:21.1	+69:30:06	0.8%	1902 / 1	10.7
6 / C4	16:50:38	21:30:00	$T_{GW} + 20.5026$	16:18:18.2	+09:59:04	5.3%	1117 / 0	–
4 / C3	16:50:46	21:30:00	$T_{GW} + 20.5037$	16:14:18.2	+30:03:36	1.5%	1117 / 0	–

Table A.7 The Observation Logs of the Mini-GWAC Follow-up of G284239 (trig. date: 2017–05–02 22:26:07.91)

mini-GWAC grid / cam ID	T_{start} 2017-05-05	T_{end} 2017-05-05	mid time (hour)	center RA (h:m:s)	center dec (deg:m:s)	$P_{GW,cov}$	N_{im} / N_{OT2}	$M_{R,OT2}$
5 / C5	12:10:29	17:09:26	$T_{GW} + 64.2304$	09:15:43.9	+69:29:34	3.2%	1196 / 0	–
7 / C6	12:10:29	17:09:36	$T_{GW} + 64.2318$	09:21:17.0	+50:29:41	0.7%	1196 / 0	–
9 / C7	12:11:12	20:09:24	$T_{GW} + 65.7361$	16:15:56.4	+29:39:59	1.7%	1913 / 0	–
3 / C4	12:15:52	14:07:41	$T_{GW} + 62.7607$	06:44:38.4	+49:45:43	6.9%	447 / 0	–
1 / C3	12:18:07	14:09:34	$T_{GW} + 62.7952$	06:35:33.2	+70:03:11	6.1%	446 / 0	–
10 / C8	12:45:41	20:09:30	$T_{GW} + 66.0243$	16:16:57.1	+10:13:56	6.2%	1775 / 30	[11.8 – 10.3]
4 / C4	14:15:38	20:09:05	$T_{GW} + 66.7704$	17:45:33.4	+10:00:59	5.2%	447 / 17	[11.8 – 9.9]
2 / C3	14:17:02	20:09:33	$T_{GW} + 66.7860$	17:41:40.8	+30:05:48	0.3%	1410 / 0	–
8 / C6	17:10:50	20:04:52	$T_{GW} + 68.1953$	12:01:27.8	+50:23:40	< 0.1%	696 / 0	–
6 / C5	19:59:14	20:09:17	$T_{GW} + 69.6354$	11:56:29.8	+69:27:40	0.8%	40 / 0	–

Table A.8 The Observation Logs of the Mini-GWAC Follow-up of G288732 (trig. date: 2017–06–08 02:01:16.492)

mini-GWAC grid / cam ID	T_{start} 2017-06-08	T_{end} 2017-06-08	mid time (hour)	center RA (h:m:s)	center dec (deg:m:s)	$P_{GW,cov}$	N_{im} / N_{OT2}	$M_{R,OT2}$ [min - max]
1 / C3	16:58:35	19:36:46	$T_{GW} + 16.2733$	01:15:34.8	+70:03:21	9.5%	633 / 4	[9.9 – 8.8]
2 / C4	17:10:44	19:31:01	$T_{GW} + 16.3267$	01:22:21.1	+49:56:18	0.5%	561 / 0	–
3 / C5	19:10:51	19:32:59	$T_{GW} + 17.3440$	03:56:21.7	+69:30:35	16.4%	89 / 4	[10.9 – 9.8]

References

Abbott, B. P., Abbott, R., Abbott, T. D., et al. 2016a, Phys. Rev. Lett., 116, 241102

Abbott, B. P., Abbott, R., Abbott, T. D., et al. 2016b, Phys. Rev. Lett., 116, 061102

Abbott, B. P., Abbott, R., Abbott, T. D., et al. 2016c, Phys. Rev. Lett., 116, 241103

Abbott, B. P., Abbott, R., Abbott, T. D., et al. 2017a, Phys. Rev. Lett., 119, 161101

Abbott, B. P., Abbott, R., Abbott, T. D., et al. 2017b, ApJ, 848, L12

Abbott, B. P., Abbott, R., Abbott, T. D., et al. 2017c, ApJ, 848, L13

Abbott, B. P., Abbott, R., Abbott, T. D., et al. 2017d, Phys. Rev. Lett., 119, 141101

Abbott, B. P., Abbott, R., Abbott, T. D., et al. 2019, ApJ, 875, 161

Alard, C. 2000, A&AS, 144, 363

Berger, E. 2014, ARA&A, 52, 43

Bertin, E., & Arnouts, S. 1996, A&AS, 117, 393

Corwin, Jr., H. G., Buta, R. J., & de Vaucouleurs, G. 1994, AJ,

108, 2128

de Mink, S. E., & King, A. 2017, ApJ, 839, L7

Eichler, D., Livio, M., Piran, T., & Schramm, D. N. 1989, Nature, 340, 126

Fan, Z., Wang, H., Jiang, X., et al. 2016, PASP, 128, 115005

Gieseke, F., Bloemen, S., van den Bogaard, C., et al. 2017, MNRAS, 472, 3101

Goldstein, A., Veres, P., Burns, E., et al. 2017, ApJ, 848, L14

Gossan, S., Ott, C., Kalmus, P., et al. 2015, in APS April Meeting Abstracts, C7.002

Huang, L., Xin, L. P., Han, X. H., Wei, J. Y., & Observatories, N. A. 2015, Optics & Precision Engineering, 23, 174

Jia, P., Zhao, Y., Xue, G., & Cai, D. 2019, AJ, 157, 250

Kotake, K., Sato, K., & Takahashi, K. 2006, Reports on Progress in Physics, 69, 971

Kulkarni, S. R. 2005, astro-ph/0510256

Leroy, N., Han, X. H., Antier, S., et al. 2017, GRB Coordinates Network, 21229, 1

Li, L.-X., & Paczyński, B. 1998, ApJ, 507, L59

Loeb, A. 2016, ApJ, 819, L21

Mahabal, A., Rebbapragada, U., Walters, R., et al. 2019, PASP, 131, 038002

Meng, X. M., Xin, L. P., Antier, S., et al. 2017, GRB Coordinates Network, 21762, 1

Mereghetti, S. 2008, A&A Rev., 15, 225

Metzger, B. D. 2017, Living Reviews in Relativity, 20, 3

Metzger, B. D., Martínez-Pinedo, G., Darbha, S., et al. 2010, MNRAS, 406, 2650

Ott, C. D. 2009, Classical and Quantum Gravity, 26, 063001

Paczynski, B. 1986, ApJ, 308, L43

Paczynski, B. 1991, Acta Astronomica, 41, 257

Perna, R., Lazzati, D., & Giacomazzo, B. 2016, ApJ, 821, L18

Sánchez, B., Domínguez R., M. J., Lares, M., et al. 2019, Astronomy and Computing, 28, 100284

Villar, V. A., Guillochon, J., Berger, E., et al. 2017, ApJ, 851, L21

Wei, J. Y., Wu, C., Leroy, N., et al. 2015, GRB Coordinates Network, 18763, 1

Wei, J., Cordier, B., Antier, S., et al. 2016, arXiv:1610.06892

Wei, J. Y., Han, X. H., Leroy, N., et al. 2017a, GRB Coordinates Network, 20369, 1

Wei, J. Y., Han, X. H., Wu, C., et al. 2017b, GRB Coordinates Network, 20490, 1

Wei, J. Y., Han, X. H., Wu, C., et al. 2017c, GRB Coordinates Network, 20695, 1

Wei, J. Y., Han, X. H., Meng, X. M., et al. 2017d, GRB Coordinates Network, 20745, 1

Wei, J. Y., Wu, C., Wang, J., et al. 2017e, GRB Coordinates Network, 20793, 1

Wei, J. Y., Han, X. H., Wu, C., et al. 2017f, GRB Coordinates Network, 20870, 1

Wenger, M., Ochsenbein, F., Egret, D., et al. 2000, A&AS, 143, 9

Xin, L. P., Wei, J. Y., Han, X. H., et al. 2017, GRB Coordinates Network, 21073, 1

Zhang, B. 2016, ApJ, 827, L31

Zhang, S.-N., Liu, Y., Yi, S., Dai, Z., & Huang, C. 2016, arXiv:1604.02537